

# Layer-by-layer deposition of zirconium oxide films from aqueous solutions for friction reduction in silicon-based microelectromechanical system devices

Jun-Fu Liu <sup>a,\*</sup>, Corina Nistorica <sup>a</sup>, Igor Gory <sup>a</sup>, George Skidmore <sup>a</sup>,  
Fadziso M. Mantiziba <sup>b</sup>, Bruce E. Gnade <sup>b</sup>

<sup>a</sup>Zyvex Corporation, 1321 N. Plano Road, Richardson, TX 75081, USA

<sup>b</sup>Department of Electrical Engineering, University of Texas at Dallas, Richardson, TX 75083, USA

Received 23 September 2004; received in revised form 8 June 2005; accepted 9 June 2005

Available online 19 July 2005

## Abstract

This work reports layer-by-layer deposition of zirconium oxide on a Si surface from aqueous solutions using the successive ionic layer adsorption and reaction technique. The process consists of repeated cycles of adsorption of zirconium precursors, water rinse, and hydrolysis. The film composition was determined by X-ray photoelectron spectroscopy. The film thickness was determined by Rutherford backscattering spectrometry, by measuring the Zr atom concentration. The average deposition rate from a 0.1 M  $Zr(SO_4)_2$  solution on a  $SiO_2/Si$  surface is 0.62 nm per cycle. Increasing the acidity of the zirconium precursor solution inhibits the deposition of the zirconium oxide film. Atomic force microscopy shows that the zirconium oxide film consists of nanoparticles of 10–50 nm in the lateral dimension. The surface roughness increased with increasing number of deposition cycles. Friction measurements made with a microelectromechanical system device reveal a reduction of 45% in the friction coefficient of zirconium oxide-coated surfaces vs. uncoated surfaces in air.

© 2005 Elsevier B.V. All rights reserved.

PACS: 81.15.Lm; 81.40.Pq; 61.14.Qp; 61.16.Ch

Keywords: Organometallic vapour deposition; Oxide; X-ray photoelectron diffraction; Atomic force microscopy

## 1. Introduction

Zirconium oxide is an important ceramic material because of its high thermal and chemical stability [1]. Zirconium oxide films have a high dielectric constant [2–4], low thermal conductivity [5–8], and excellent wear resistance [9–11].

Current deposition methods of ultra-thin films of zirconium oxide include gas-phase [12–19], and liquid-phase deposition [20–25]. Gas-phase deposition techniques such as chemical vapor deposition, atomic layer deposition, and sputtering, usually require high substrate temperature and expensive vacuum deposition systems. Liquid-phase deposition techniques such as sol–gel [26–28], chemical bath

deposition [29], and successive ionic layer adsorption and reaction (SILAR) [29], work at ambient temperature and atmosphere. The liquid phase deposition techniques are simple and low cost. The precursors used for liquid phase deposition are normally more environmentally benign than those used for gas phase deposition [30].

As compared with other liquid phase deposition techniques, the SILAR method allows control of the film thickness at the nanometer scale because SILAR proceeds layer-by-layer. Each SILAR cycle consists of four steps; 1) the adsorption of cations on the Si surface, 2) water rinse to remove unadsorbed cations, 3) the reaction of anions with the adsorbed cation precursors, and 4) water rinse to remove unreacted anions. Multilayers are deposited by repeating the cycle.

The SILAR method can be used to deposit sulfide and oxide thin films [31]. Park et al. used the SILAR method

\* Corresponding author. Present address: Department of Chemistry, University of New Hampshire, Durham, NH 03824, USA.

E-mail address: [j.f.liu@unh.edu](mailto:j.f.liu@unh.edu) (J.-F. Liu).

to deposit  $\text{ZrO}_2$  on a  $\text{Si}_3\text{N}_4/\text{Si}$  substrate from aqueous solutions of  $\text{Zr}^{4+}$  ions and  $\text{OH}^-$  ions [32]. In this paper, we report the deposition of zirconium oxide thin films on Si surfaces using the SILAR method, the characterization of the deposited film, and its use as a surface coating for silicon-based microelectromechanical system (MEMS) for friction reduction.

## 2. Experimental details

### 2.1. Chemicals

The precursor solutions used for the SILAR deposition were zirconium sulfate ( $\text{Zr}(\text{SO}_4)_2$ , 99.9%, 40 wt.% solution in water, Aldrich), and 0.1 M sodium hydroxide (NaOH, 99.99%, semiconductor grade, Aldrich). Zirconium sulfate solutions were used within 48 h after preparation. All solutions were prepared using reagent grade water (A.C.S. reagent, Aldrich). The solution used to clean the silicon substrates was a mixture of concentrated sulfuric acid ( $\text{H}_2\text{SO}_4$ , 95–98%, Aldrich) and hydrogen peroxide ( $\text{H}_2\text{O}_2$ , 35 wt.% solution in water, Aldrich) (7:3 volume proportions of concentrated  $\text{H}_2\text{SO}_4$ :35%  $\text{H}_2\text{O}_2$ ). This cleaning solution is often referred to as piranha in the semiconductor industry, and is used to remove organic contamination from silicon wafers, leaving a thin chemical oxide on the surface of the silicon wafer.

### 2.2. Substrates

The Si substrates (1.5 cm  $\times$  1.5 cm) were cut from Si(100) wafers (Boron-doped, single side polished, 0.01–0.02  $\Omega$ -cm, 500–550  $\mu\text{m}$  thick, MEMC Electronic Materials Inc.). A hydrophilic  $\text{SiO}_2/\text{Si}$  surface was obtained by immersing the Si wafers in a hot piranha solution at 80–120  $^\circ\text{C}$  for 30 min, followed by rinsing with reagent grade water for  $\sim 20$  s. A very thin hydrophilic  $\text{SiO}_2$  film of  $\sim 1.3$  nm was formed on the Si surface after it was cleaned with piranha solutions [33].

### 2.3. SILAR deposition

The SILAR deposition was performed at 24–26  $^\circ\text{C}$  using a combination of a four channel programmable Teflon valve perfusion system (Automate Scientific Inc., San Francisco, CA) and a spin coater (Model P-6708D, Specialty Coating Systems, Indianapolis, IN). The SILAR deposition of zirconium oxide films started with adsorption from the 0.1 M  $\text{Zr}(\text{SO}_4)_2$  solutions and ended with adsorption from the 0.1 M NaOH solution. The adsorption time for both solutions was 20 s. The rinse time was 20 s. Multilayers of the zirconium oxide film were built up by repeating the deposition cycle. For all depositions, the speed of the spin coater was kept constant at 1300 revolutions per minute for each adsorption and rinse.

### 2.4. Atomic force microscopy (AFM)

The surface morphology of the zirconium oxide films was imaged with a NanoScope IIIa Multimode AFM (Digital Instruments, Santa Barbara, CA). Tapping mode measurements were carried out with Ultrasharp noncontact silicon cantilevers (MikroMasch, Tallinn, Estonia) with a typical length of 125  $\mu\text{m}$ , typical resonance frequency of 325 kHz and typical force constants of 40 N/m. The scan rate was 1 Hz. The AFM was calibrated using an Ultrasharp silicon grating (TGZ01, NT-MDT, pitch depth 25.5 nm, pitch size 3.0  $\mu\text{m}$ ).

### 2.5. X-ray photoelectron spectroscopy (XPS)

Surface chemical analysis was done by X-ray photoelectron spectroscopy (XPS) using a twin anode Al- $\text{K}_\alpha$  X-ray source. For each sample, a survey scan was first taken over the entire spectral range (0–1400 eV) at a pass energy of 200 eV. Expansion regions were done at a pass energy of 20 eV. All data were acquired at normal incidence to the sample surfaces.

### 2.6. Rutherford backscattering spectrometry (RBS)

RBS was used to determine the thickness of the zirconium oxide films. The RBS analysis was conducted using a 2.0 MeV  $\text{He}^+$  beam incident normal to the sample surface, with a scattering angle of 150 $^\circ$  and a detection solid angle of  $1.14 \times 10^{-3}$  sr. The physical thickness of the films, as determined by RBS, assumes a density of 4.1 g/cm $^3$ . The areal density of zirconium atoms is accurate to <10%.

### 2.7. Friction measurement

A silicon on insulator (SOI)-based thermal MEMS actuator was used for direct measurement of static friction between two surfaces. As shown in Fig. 1a, the interacting surfaces are 50- $\mu\text{m}$ -thick side-walls fabricated using Deep Reactive Ion Etching. Using this thermal MEMS actuator, frictional behavior between two surfaces can be studied under different environmental conditions by placing the device in an environmental chamber where humidity can be controlled. Two thermal bent beam actuators apply the normal force and the tangential force to obtain the relative motion of the two surfaces. A bias voltage applied to the lower amplified bent beam actuator provides the normal force that will clamp the central beam symmetrically. Another bent beam thermal actuator, attached to the central beam, exerts the tangential force required to overcome the static friction force and provide motion between the central beam and the clamps. Fig. 1b,c show the thermal MEMS actuator in the zero voltage position and in the actuated position, respectively. The friction force data were collected at zero relative humidity, in a dry nitrogen atmosphere, down to a pressure of 100 mm Hg and compared to data collected for the friction

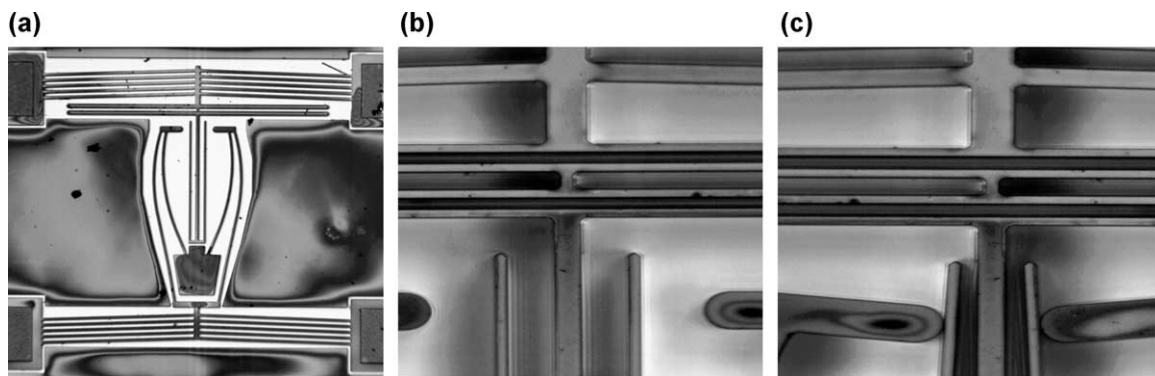


Fig. 1. Friction measurement device: (a) SOI-based 50  $\mu\text{m}$  thermal MEMS actuator, (b) zero voltage position, (c) actuated position.

coefficient in air at ambient relative humidity of  $50 \pm 5\%$ . In all the experiments the normal force varied between 5  $\mu\text{N}$  and 50  $\mu\text{N}$  and the sliding speed was 12.5  $\mu\text{m/s}$ . All the experiments were performed at room temperature. The surface cleaning of the MEMS actuator and deposition procedures on its surface were the same as those used for bare Si substrates.

### 3. Results and discussion

#### 3.1. XPS

Fig. 2 shows the results of the XPS analysis of the deposited zirconium oxide film on  $\text{SiO}_2/\text{Si}$ . Peaks of Si, Zr, O, and C were observed in the survey spectrum in Fig. 2a. Fig. 2b shows the  $\text{Zr}_{3d5/2}$  and  $\text{Zr}_{3d3/2}$  peaks at binding energies of 184.2 eV and 186.6 eV. The binding energy of the  $\text{Zr}_{3d5/2}$  peak at 184.2 eV is larger than the reported binding energy of 182.2 eV for zirconia [34], and that of 181.8 eV for hydrous zirconia [35,36]. This shift of the binding energy to a higher value can be attributed to stronger Zr–O bond polarization [37]. However, it is comparable to 183.6 eV for the  $\text{Zr}_{3d5/2}$  photoelectron peak from zirconium hydroxide, suggesting that the deposited film contains Zr–OH.

The XPS data shows evidence of contamination from carbon. The peak between 284 eV and 288 eV in Fig. 2c was fit as three peaks at 286.0 eV (C–OH), 284.5 eV (C–H), and 288.2 eV (C=O), implying contamination of hydrocarbon (C–C), alcohol or ether (C–O), and organic acids (C=O). The peak between 531 eV and 534 eV in Fig. 2d represents the  $\text{O}_{1s}$  peak. It was fit as two peaks at 533.6 eV and 532.1 eV, which corresponds to Si–O bond and the Zr–OH bond, respectively [38–41]. The oxygen peak also shows contributions from the carbon contamination, because the  $\text{O}_{1s}$  peaks of –OH, C–O, and C=O are also within the range between 531 eV and 534 eV. The  $\text{Si}_{2p}$  peaks in Fig. 2e, at 99.9 eV and 103.4 eV, correspond to the Si–Si and the Si–O bond, respectively. The presence of the Si peaks is consistent with the  $\text{O}_{1s}$  peak at 533.6 eV of the Si–O bond, coming from the  $\text{SiO}_2/\text{Si}$  surface below the zirconium oxide film.

We believe that the deposition of zirconium oxide on  $\text{SiO}_2/\text{Si}$  is initiated by the adsorption of Zr cations on the surface silanol groups. Silanol groups are present on the silica surface in aqueous solutions and their density is approximately  $4/\text{nm}^2$  [42]. The O atoms of the silanol groups have a partial negative charge and Zr cations can adsorb on the silanol groups via ion–dipole interactions. Reaction of the adsorbed Zr cations with 0.1 M NaOH during the hydrolysis step results in the deposition of zirconium oxide on the  $\text{SiO}_2/\text{Si}$  surface.

#### 3.2. RBS

To determine the film thickness and the atomic ratio of Zr/O, the zirconium oxide films were analyzed using Rutherford Backscattering Spectroscopy. From the RBS measurement, the atomic ratio of Zr/O of the deposited zirconium oxide film is determined to be 1:2.6. The change of thickness, as calculated by determining the zirconium atoms/ $\text{cm}^2$ , with deposition cycles of zirconium oxide films is shown in Fig. 3. When the  $\text{Zr}(\text{SO}_4)_2$  precursor solution was used, an induction period was observed as shown in Fig. 3. There was little deposition for <10 SILAR cycles. After 10 SILAR cycles, the film thickness increased linearly with deposition cycles. The average deposition rate of 50 SILAR cycles is 0.62 nm per cycle.

The acidity of the precursor solutions has a strong effect on the deposition rate. When the Zr precursor solution was changed from 0.1 M  $\text{Zr}(\text{SO}_4)_2$  to 0.1 M  $\text{Zr}(\text{SO}_4)_2 + 0.1$  M  $\text{H}_2\text{SO}_4$ , as shown in Fig. 3 the deposition rate was decreased to 0.1 nm per cycle. The decrease of the deposition rate can be attributed to the competition of the adsorption of  $\text{H}^+$  ions with Zr cations on the surface silanol groups on  $\text{SiO}_2/\text{Si}$ , which can result in a decrease of the surface density of the adsorbed Zr cations, and thus a decreased deposition rate.

#### 3.3. AFM

Fig. 4 shows the AFM images of the surface morphology of the zirconium oxide films on  $\text{SiO}_2/\text{Si}$ . As can be seen from Fig. 4a, the  $\text{SiO}_2/\text{Si}$  surface is reasonably smooth. As

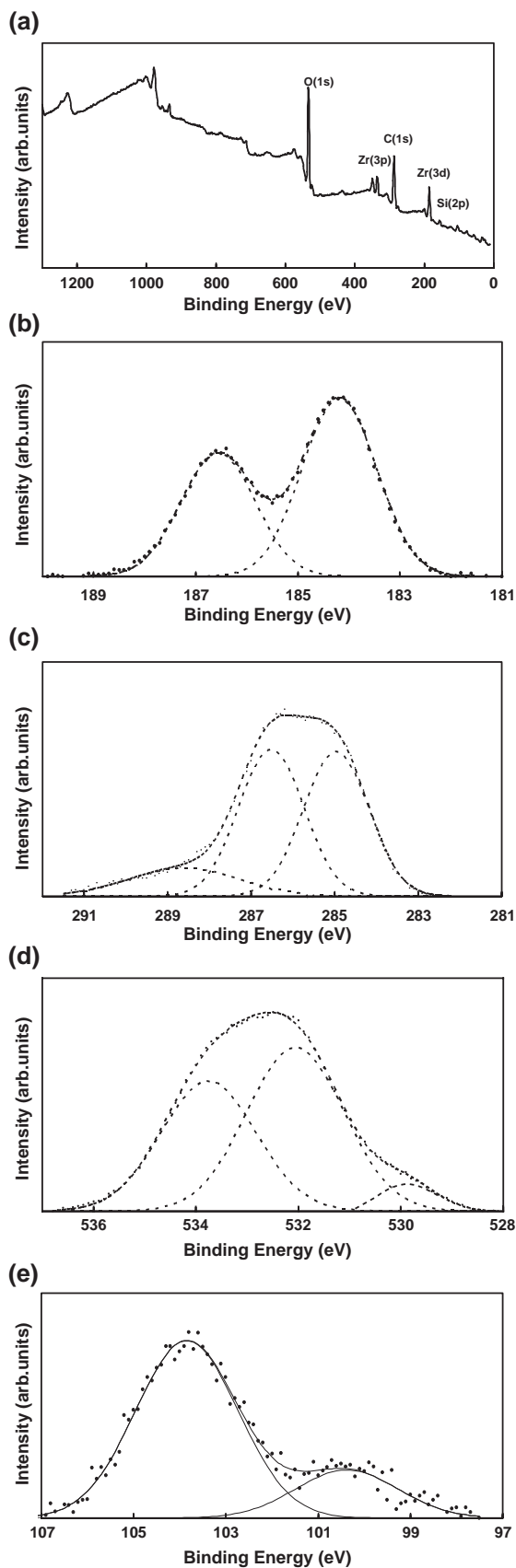


Fig. 2. X-ray photoelectron spectra of a zirconium oxide film of 30 deposition cycles from 0.1 M  $Zr(SO_4)_2$  on  $SiO_2/Si$ : (a) survey scan, (b)  $Zr_{3d}$ , (c)  $C_{1s}$ , (d)  $O_{1s}$ , and (e)  $Si_{2p}$ .

the number of SILAR cycles increased, 3-dimensional features formed on the surface. At 5 SILAR cycles of deposition from 0.1 M  $Zr(SO_4)_2$ , features of 10–50 nm in the lateral dimension were observed on the  $SiO_2/Si$  surface (Fig. 4b). These features grew in size and density with deposition cycles (Fig. 4c). The corresponding cross-sectional analysis shows similar changes of the surface morphology with deposition cycles. Similar to the surface features in Fig. 4b, circular features of 10–50 nm were observed on  $SiO_2/Si$  (Fig. 4d) at 5 SILAR cycles of deposition from 0.1 M  $Zr(SO_4)_2 + 0.1$  M  $H_2SO_4$ . These features also increased in size and density with the number of deposition cycles (Fig. 4e). The zirconium oxide films of 50 SILAR cycles (Fig. 4c and e) were much rougher than those of 5 SILAR cycles (Fig. 4b and d).

Formation of 3-dimensional features as observed in Fig. 4(b–e) can be attributed to partial coverage of adsorbed Zr cations on the  $SiO_2/Si$  surface. Because of the competition of the adsorption of Zr cations with  $H^+$  ions for the silanol groups on the  $SiO_2/Si$  surface, the adsorption of Zr cations could not reach full coverage. The SILAR deposition proceeds only on those sites covered with adsorbed Zr cations, resulting in the formation of the 3-dimensional features which grew with the number of SILAR cycles.

### 3.4. Friction coefficient

Curves (a, b) in Fig. 5 represent the waveform applied on the lower and upper thermal MEMS actuators shown in Fig. 1a. The voltage on the lower actuator was kept constant, so that the normal force would be constant on the surface, while the voltage on the second actuator was ramped up so that the elastic force exerted by the upper spring would be increased gradually. The tangential frictional force is defined as the force that initiates sliding between the two contacting surfaces.

The value of the normal force applied on the surface was calculated as being equal to the elastic force from the central vertical spring, while the static friction force was determined by equating the friction force to the elastic force from the upper horizontal spring. The elastic forces of the springs

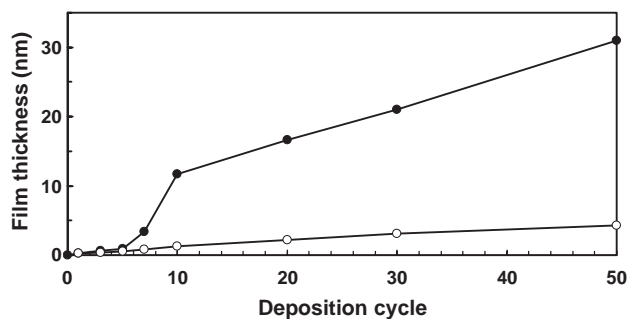


Fig. 3. Increase of film thickness of zirconium oxide with deposition cycles on  $SiO_2/Si$ . Precursor solutions (●) 0.1 M  $Zr(SO_4)_2$ , (○) 0.1 M  $Zr(SO_4)_2 + 0.1$  M  $H_2SO_4$ . The value of the film thickness is based on a formula of  $ZrO_2 \cdot 0.6H_2O$ .

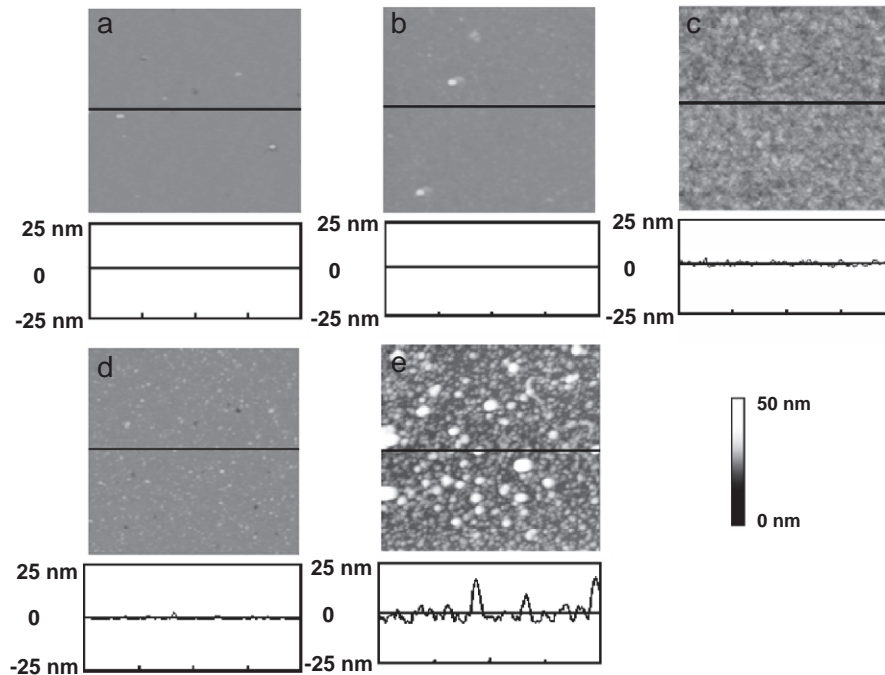


Fig. 4. AFM height images ( $1 \mu\text{m} \times 1 \mu\text{m}$ ) of zirconium oxide on  $\text{SiO}_2/\text{Si}$  and cross-section curves. (a)  $\text{SiO}_2/\text{Si}$ , (b) 5 cycles deposited from 0.1 M  $\text{Zr}(\text{SO}_4)_2$ , (c) 50 cycles deposited from 0.1 M  $\text{Zr}(\text{SO}_4)_2$ , (d) 5 cycles deposited from 0.1 M  $\text{Zr}(\text{SO}_4)_2+0.1 \text{ M H}_2\text{SO}_4$ , and (e) 50 cycles deposited from 0.1 M  $\text{Zr}(\text{SO}_4)_2+0.1 \text{ M H}_2\text{SO}_4$ .

$F_{\text{el},n}$  and  $F_{\text{el},t}$  were calculated by knowing the displacement of the springs  $\delta_n$  and  $\delta_t$ , and the spring constants  $k_n$  and  $k_f$  as follows

$$F_{\text{el},n} = k_n \delta_n \quad (1)$$

$$F_{\text{el},t} = k_f \delta_t. \quad (2)$$

The values of the spring constants were determined using finite element analysis. Uncertainties in the material parameters used are taken into account in the final error analysis. The displacement of the springs was measured using a MEMS Motion Analyzer (MMA) with a resolution of 10 nm at the magnification used in the measurements. High temporal and spatial resolution of the

MMA enables the detection of small motions associated with slipping.

Curves (c, d) in Fig. 5 show typical tangential force and normal force values vs. time obtained while the corresponding waveforms (curve a and curve b) were applied to the thermal actuators. Stick-slip behavior was observed in all cases, for uncoated as well as for coated devices. For a limited range of the normal force  $F_N > 0$ , the relation between the friction force  $F_F$  and the normal force  $F_N$  can be approximated by a linear equation,

$$F_F = \mu_s (F_N + F_A) \quad (3)$$

where  $F_A$  is the adhesion force contributing to the total load and  $\mu_s$  is the static friction coefficient.

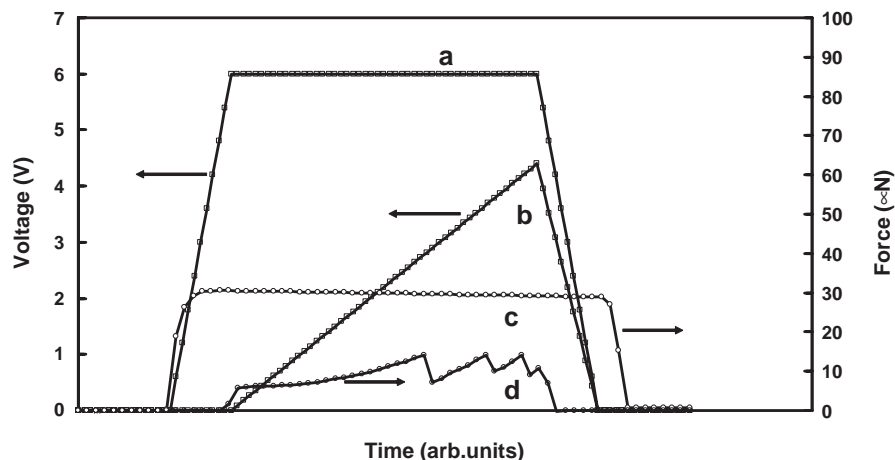


Fig. 5. Waveforms applied on the two thermal actuators of the friction micro tester (a, b) and typical normal loading force and tangential friction force (c, d).

Fig. 6 shows the relation between the friction force measured at the onset of slip and the measured normal force of the uncoated MEMS device (Fig. 6a) and the MEMS devices coated with ZrO<sub>2</sub> films of 10 SILAR cycles deposited from 0.1 M Zr(SO<sub>4</sub>)<sub>2</sub> (Fig. 6b) and 0.1 M Zr(SO<sub>4</sub>)<sub>2</sub>+0.1 M H<sub>2</sub>SO<sub>4</sub> (Fig. 6c). As can be seen from the data, linear relationships exist between the friction and the normal force. The change of friction coefficient was obtained from the slope by fitting the data to a straight line. The change in the coefficient of friction as a function of ambient pressure is shown in Fig. 7. At pressures smaller than 0.5 mm Hg, the friction coefficient of the device coated with the 10 SILAR cycles of the ZrO<sub>2</sub> film deposited from 0.1 M Zr(SO<sub>4</sub>)<sub>2</sub> precursor is lower than that of the uncoated MEMS device. At pressures larger than 0.5 mm Hg, however, there is little difference in the friction coefficient.

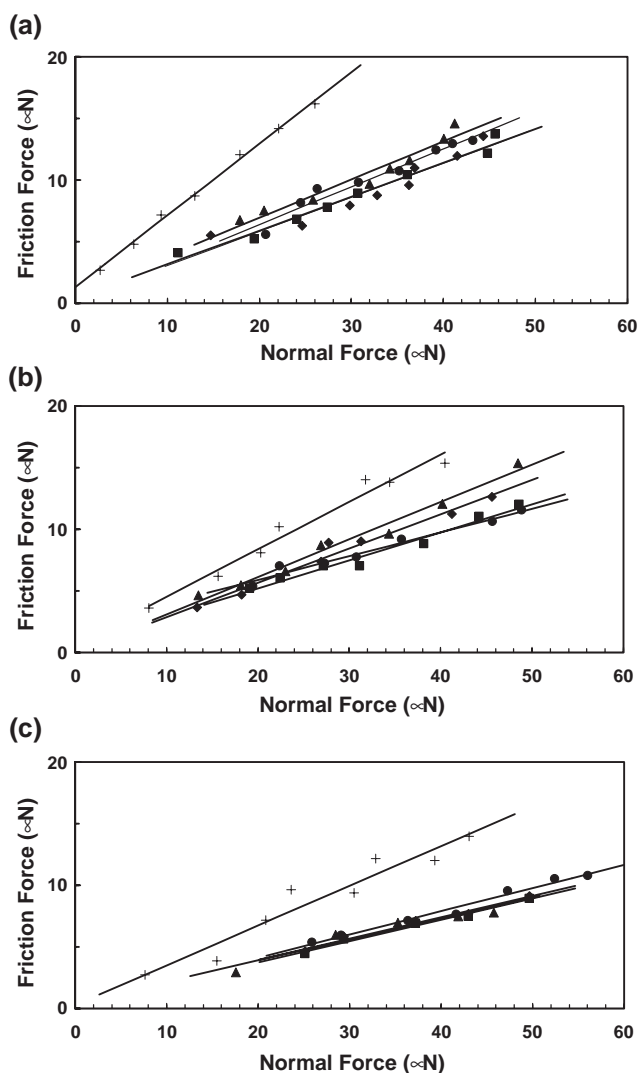


Fig. 6. Plot of friction force vs. normal force: (a) uncoated Si device, (b) Si device coated with zirconium oxide of 10 cycles deposited from 0.1 M Zr(SO<sub>4</sub>)<sub>2</sub>, (c) Si device coated with zirconium oxide of 10 cycles deposited from 0.1 M Zr(SO<sub>4</sub>)<sub>2</sub>+0.1 M H<sub>2</sub>SO<sub>4</sub>. (+) in air, (●) 0.1 mm Hg, (◆) 0.2 mm Hg, (■) 0.5 mm Hg, (▲) 1 mm Hg.

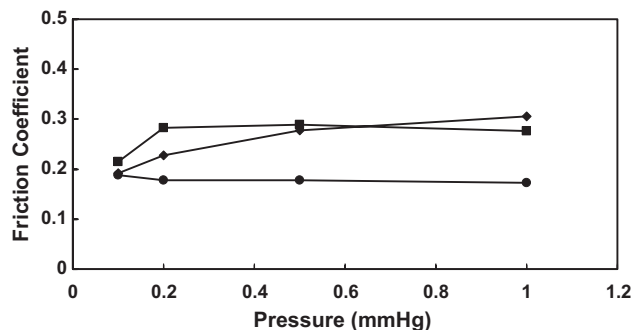


Fig. 7. Plot of friction coefficient vs. pressure: (■) uncoated MEMS device, (◆) Si device coated with zirconium oxide of 10 cycles deposited from 0.1 M Zr(SO<sub>4</sub>)<sub>2</sub>, and (●) Si device coated with zirconium oxide of 10 cycles deposited from 0.1 M Zr(SO<sub>4</sub>)<sub>2</sub>+0.1 M H<sub>2</sub>SO<sub>4</sub>.

For the zirconium oxide film of 10 cycles deposited from 0.1 M Zr(SO<sub>4</sub>)<sub>2</sub>+0.1 M H<sub>2</sub>SO<sub>4</sub>, there was almost no difference in the friction coefficient from the uncoated MEMS device at 0.1 mm Hg. In contrast, the static friction coefficient decreased by about 37% at a pressure larger than 0.2 mm Hg. The friction coefficient can be affected by surface roughness, rolling of zirconium oxide nanoparticles on the surface, and adhesion force. As can be seen from Fig. 4, the coated Si surface is rougher than the uncoated Si surface. It is known that a relatively small increase of the surface roughness is sufficient to reduce the adhesion of the surfaces [43–46]. The decrease of the friction coefficient in Fig. 7 can be attributed to the rougher surface of the coated surface compared to the uncoated surface. Secondly, the presence of nanoparticles on the coated surfaces could result in a change from sliding friction to rolling friction of the two surfaces, thus decreasing the friction between the two surfaces.

We found that the friction coefficient of both uncoated and coated MEMS devices when measured in air is much higher than at pressures of 0.1–1 mm Hg. The friction coefficient of the uncoated MEMS device measured in air was 0.586 in contrast to 0.215 at 0.1 mm Hg. After coating with 10 cycles of ZrO<sub>2</sub> from 0.1 M Zr(SO<sub>4</sub>)<sub>2</sub> and 0.1 M Zr(SO<sub>4</sub>)<sub>2</sub>+0.1 M H<sub>2</sub>SO<sub>4</sub>, the friction coefficient of the MEMS devices in air decreased from 0.384 and 0.323 to 0.192 and 0.188 at 0.1 mm Hg, a decrease of 45% in the friction coefficient in air as compared with the uncoated MEMS device.

#### 4. Conclusions

Thin zirconium oxide films were deposited on the SiO<sub>2</sub>/Si surface layer-by-layer using the SILAR method. The SILAR process, which comprises cycles of adsorption of zirconium precursors, rinsing with water, and hydrolysis in an alkaline media, offers precise control of the film growth rate. The application of the combination of an automatic perfusion system with a spin coater provides a useful method for deposition of thin films using the SILAR

process. The friction coefficient of the MEMS device in air can be decreased by 45% by the presence of a zirconium oxide film, demonstrating potential applications for friction reduction in MEMS devices.

### Acknowledgment

This work was supported in part by the United States Department of Commerce, NIST-ATP Award #70NANB1H3021.

### References

- [1] K. Izumi, M. Murakami, T. Deguchi, A. Morita, *J. Am. Ceram. Soc.* 72 (1989) 1465.
- [2] G.D. Wilk, R.M. Wallace, J.M. Anthony, *J. Appl. Phys.* 89 (2001) 5243.
- [3] M.J. Biercuk, D.J. Monsma, C.M. Marcus, J.S. Becker, R.G. Gordon, *Appl. Phys. Lett.* 83 (2003) 2405.
- [4] D.H. Kuo, C.H. Chien, *Thin Solid Films* 429 (2003) 40.
- [5] A.S. Kao, C. Hwang, *J. Vac. Sci. Technol., A, Vac. Surf. Films* 8 (1990) 3289.
- [6] M. Shane, M.L. McCartney, *J. Mater. Sci.* 25 (1990) 1537.
- [7] A.S. Kao, G.L. Gorman, *J. Appl. Phys.* 67 (1990) 3826.
- [8] M. Agarwal, M.R. De Guire, A.H. Heuer, *J. Am. Ceram. Soc.* 80 (1997) 2967.
- [9] B. Basu, R.G. Vitchev, J.P. Cellis, O.V. Der Biest, *Acta Mater.* 48 (2000) 2461.
- [10] T.E. Fischer, M.P. Anderson, S. Jahanmir, R. Saher, *Wear* 124 (1988) 133.
- [11] W. Morales, D.H. Buckley, *Wear* 123 (1988) 345.
- [12] M. Houssa, A. Stesmans, M. Naili, M.M. Heyns, *Appl. Phys. Lett.* 77 (2000) 1381.
- [13] M. Copel, M. Gribelyuk, E. Gusev, *Appl. Phys. Lett.* 76 (2000) 436.
- [14] M.A. Cameron, S.M. George, *Thin Solid Films* 348 (1999) 90.
- [15] D.M. Hausmann, E. Kim, J. Becker, R.G. Gordon, *Chem. Mater.* 14 (2002) 4350.
- [16] J.P. Chang, Y.-S. Lin, S. Berger, A. Kepten, R. Bloom, S. Levy, *J. Vac. Sci. Technol., B* 19 (2001) 2137.
- [17] M.A. Boorst, W.Y. Lee, Y. Zhang, P.K. Liaw, *J. Am. Ceram. Soc.* 30 (1997) 1591.
- [18] P. Yashar, J. Rechner, M.S. Wong, W.D. Sproul, S.A. Barnett, *Surf. Coat. Technol.* 333 (1997) 94.
- [19] L.S. Wang, S.A. Barnett, *J. Electrochem. Soc.* 139 (1992) 1134.
- [20] T. Niesen, M.R. De Guire, J. Bill, F. Aldinger, M. Ruhle, A. Fischer, F.C. Jentoft, R. Schlogl, *J. Mater. Res.* 14 (1999) 2464.
- [21] Y. Gao, Y. Masuda, H. Ohta, K. Koumoto, *Chem. Mater.* 16 (2004) 1702.
- [22] H. Shin, M. Agarwal, M.R. De Guire, *Acta Mater.* 46 (1998) 801.
- [23] A.D. Poli, T. Wagner, A. Fischer, G. Weinberg, F.C. Jentoft, R. Schlogl, M. Ruhle, *Thin Solid Films* 379 (2000) 122.
- [24] T. Yao, T. Inui, A. Ariyoshi, *J. Am. Ceram. Soc.* 79 (1996) 3329.
- [25] T. Yao, *J. Mater. Res.* 13 (1998) 1091.
- [26] M. Shane, M.L. McCartney, *J. Mater. Sci.* 25 (1990) 1537.
- [27] Y. Yu, X. Wang, Y. Cao, X. Hu, *Appl. Surf. Sci.* 72 (2001) 260.
- [28] J.F. Quinson, C. Chino, A.M. De Beccdelievre, C. Guizard, M. Brunel, *J. Mater. Sci.* 31 (1996) 5179.
- [29] T.P. Niesen, M.R. De Guire, *Solid State Ionics* 151 (2002) 61.
- [30] M. Yoshimura, W.L. Suchanek, K. Byrappa, *MRS Bull.* 25 (2000) 17.
- [31] T. Niesen, M.R. De Gure, *J. Electroceram.* 6 (2001) 169.
- [32] S. Park, B.L. Clark, D.A. Keszler, J.P. Bender, J.F. Wager, T.A. Reynolds, G.S. Herman, *Science* 297 (2002) 65.
- [33] R.J. Collins, N.S. Chaim, *Langmuir* 11 (1995) 2322.
- [34] W. Qi, R. Nieh, B.H. Lee, L. Kang, Y. Jeon, K. Onish, T. Ngai, S. Banerjee, J.C. Lee, *IEEE Proceeding Technical Digest*, 1999, p. 145.
- [35] C. Huang, Z. Tong, Z. Zhang, *J. Am. Ceram. Soc.* 84 (2001) 1637.
- [36] B.-O. Cho, S. Lao, L. Sha, J.P. Chang, *J. Vac. Sci. Technol., A, Vac. Surf. Films* 19 (2001) 2751.
- [37] G. Alberti, U. Costantino, G. Marletta, O. Puglisi, S. Pignataro, *J. Inorg. Nucl. Chem.* 43 (1981) 3329.
- [38] J. Sefcik, A.V. McCormick, *Catal. Today* 35 (1997) 205.
- [39] J.J. Chambers, G.N. Parsons, *Appl. Phys. Lett.* 77 (2000) 2385.
- [40] G. Lucovsky, G.B. Rayner, D. Kang, G. Appel, R.S. Johnson, Y. Zhang, D.E. Ade, H. Sayers, J.L. Whitten, *Appl. Phys. Lett.* 79 (2001) 1775.
- [41] M.J. Guittet, J.P. Crocombette, M. Gautier-Soyer, *Phys. Rev., B* 63 (2001) 125117.
- [42] R.K. Iler, *The Chemistry of Silica*, Wiley, New York, 1979.
- [43] K.N.G. Fuller, D. Tabor, *Proc. R. Soc. Lond., A* 345 (1975) 327.
- [44] D. Maugis, *J. Adhes. Sci. Technol.* 10 (1996) 161.
- [45] B. Bhushan, *Principles and Applications of Tribology*, Wiley, NewYork, 2002.
- [46] B. Bhushan, *J. Vac. Sci. Technol., B* 21 (2003) 2262.